Article

Not peer-reviewed version

Haploid *Armillaria ostoyae* Cells as Hypersensitive Biosensors Reveal Asymmetric Volatile-Mediated Reprogramming During Airborne Interaction with *Trichoderma atroviride*

Omar Languar [†], Simang Champramary [†], Orsolya Kedves, András Szekeres, Attila Szűcs, Nóra Tünde Lange-Enyedi, Boris Indic, Sándor Kiss-Vetráb, Gábor Nagy, Árpád Bányi, Csaba Vágvölgyi, Younes Rezaee Danesh, László Kredics, György Sipos [*]

Posted Date: 29 April 2026

doi: 10.20944/preprints202604.2000.v1

Keywords: volatile organic compounds (VOCs); fungal interspecies interactions; *Trichoderma atroviride*; *Armillaria ostoyae*; secondary metabolism regulation; multi-omics integration

 doi:10.20944/preprints202604.2000.v1

Article

Haploid *Armillaria ostoyae* Cells as Hypersensitive Biosensors Reveal Asymmetric Volatile-Mediated Reprogramming During Airborne Interaction with *Trichoderma atroviride*

Omar Languar [1,2,†], Simang Champramary [1,†], Orsolya Kedves [2], András Szekeres [2], Attila Szűcs [3], Nóra Tünde Lange-Enyedi [1], Boris Indic [1], Sándor Kiss-Vetráb [2], Gábor Nagy [4], Árpád Bányi [5], Csaba Vágvölgyi [2], Younes Rezaee Danesh [6], László Kredics [2] and György Sipos [1,*]

[1] Functional Genomics and Bioinformatics Group, Faculty of Forestry, University of Sopron, Sopron, Hungary
[2] Department of Biotechnology and Microbiology, Faculty of Science and Informatics, University of Szeged, Szeged, Hungary
[3] University of Innsbruck, Department of Zoology, Innsbruck, Austria
[4] HUN-REN Biological Research Centre, Institute of Genetics, Mutagenesis and Carcinogenesis Research Group, Szeged, Hungary
[5] Pannon-Trade Ltd., Győr, Hungary
[6] Department of Plant Protection, Faculty of Agriculture, Van Yuzuncu Yil University, Van, Türkiye
* Correspondence: sipos.gyorgy@uni-sopron.hu
† These authors contributed equally to this work.

Abstract

Volatile organic compound (VOC)-mediated communication between distinct fungal colonies is a crucial yet poorly understood aspect of interspecies interactions. We investigated the airborne interactions between *Trichoderma atroviride* (SZMC 24276) and haploid *Armillaria ostoyae* (SZMC 23085) hyphae using an in vitro face-off system that combined transcriptomic and gas chromatography-mass spectrometry (GC-MS) analyses. Distinct temporal VOC profiles were observed, including the early accumulation of the constitutively produced 6-pentyl-α-pyrone (6-PP) and the later appearance of 2-heptanone from *T. atroviride*, as well as the production of an interaction-specific cadinane-type sesquiterpene in *A. ostoyae*. Multi-omics integration revealed a direct coupling between transcriptional regulation and volatile output, with suppression of C8 signaling compounds such as 1-octen-3-ol and non-ribosomal peptide synthetase-associated pathways in *T. atroviride* under volatile exposure. In contrast, *A. ostoyae* exhibited extensive transcriptional reprogramming characterized by oxidative stress responses, detoxification pathways, and activation of terpene biosynthetic clusters. These findings indicate that *T. atroviride* constitutively produces 6-PP as a broad-spectrum volatile irritant and modulates its secondary metabolism in a context-dependent manner, while *A. ostoyae* responds to volatile cues through stress-associated and defensive mechanisms. Overall, this study demonstrates that VOCs function as active regulators of interactions before physical contact, shaping both metabolic and transcriptional responses, and highlights their potential role in *Trichoderma*-based biocontrol strategies against *Armillaria*.

Keywords: volatile organic compounds (VOCs); fungal interspecies interactions; *Trichoderma atroviride*; *Armillaria ostoyae*; secondary metabolism regulation; multi-omics integration

1. Introduction

Among the most harmful plant-pathogenic fungi, *Armillaria* species are known for causing root rot diseases in a wide range of woody plants [1,2]. In forest ecosystems, infections caused by

 doi:10.20944/preprints202604.2000.v1

Armillaria species can have detrimental effects including significant tree mortality and reduced plant fitness. A primary pathogen of coniferous trees, *Armillaria ostoyae* is a facultative necrotrophic species that favors coniferous habitats [3]. After colonizing the cambium in living roots, the fungus begins to cause necrotic lesions underneath it. After killing the cambium, it also absorbs the dead tissues and uses it as a food source to attack nearby healthy trees [1,4]. While mycelia and rhizomorphs of *Armillaria* species share similar functions, it is the specialized rhizomorph that penetrates deep into the soil, allowing them to effectively colonize and invade newly planted trees. Therefore, it can take decades to completely eradicate a soil infestation by *Armillaria* [5,6].

Unfortunately, conventional methods of protecting forests and chemical control strategies based on fungicides have many disadvantages [7]. Yet, biocontrol strategies present a possibly superior choice since they use microorganisms such as members of the genus *Trichoderma* to terminate plant diseases [8]. This approach focuses on safeguarding both human health and the environment by decreasing the amount of pesticides. It guarantees the absence of pesticide residues, making it a more sustainable choice. Furthermore, numerous biocontrol agents (BCAs) successfully protect plants from various diseases caused by pathogens while also enhancing plant growth, resulting in higher yields [9,10].

Species in the mycoparasitic genus *Trichoderma* are known for their impressive adaptability and survival capacity, which is why they are commonly found in soil environments. They employ several biocontrol mechanisms, including mycoparasitic interactions with fungi that cause diseases in plants [11,12].

In our previous study, *Trichoderma atroviride* showed strong antagonistic effects against the haploid derivative of *A. ostoyae*. To better understand this interaction, we examined the transcriptomes of both *A. ostoyae* (AO) and *T. atroviride* (TA) in in vitro dual culture assays. This analysis aimed to explore the mycoparasitic molecular mechanism used by *Trichoderma* for antagonism and the defense strategies employed by *Armillaria* [11].

Meanwhile, preliminary transcriptomic data involving the same isolates sharing only airspace, not in direct physical contact, suggested that airborne communication may already occur between them. In our current study, we examined these airborne interactions more closely using a multi-omics approach. By combining RNA sequencing, GC-MS analysis of volatile compounds, and biosynthetic gene cluster annotation, we aimed to capture both transcriptional and metabolic changes during the interaction. To separate the impacts of airborne signaling from direct contact, we used a shared-airspace co-culture system, allowing the two fungi to communicate through volatiles while preventing metabolite exchange through the medium. This setup revealed that the interaction is not symmetrical: each species responds differently at the transcriptional level. We also observed interaction-specific changes in secondary metabolism, including a reduction in TA VOC production in co-culture and mode-dependent regulation of biosynthetic gene clusters.

Our current approach is based on the study of the effects on haploid AO cells, which may act as hypersensitive native biosensors that respond rapidly to aggressive volatiles released by the potential invasive mycoparasitic partner. Here we aim to identify the molecular basis of hypersensitivity and responsiveness in haploid *Armillaria* cells, explore the chemicals released by *Trichoderma* cells that elicit this response, and investigate the possible defense mechanisms including also the responsive volatiles of haploid AO cells.

The interaction between AO and TA, involving volatile organic compounds (VOCs), is a prime example of the complex network of biochemical signalling and ecological interactions between fungi. Our current focus is on understanding the basis of VOC production in each species and the VOC-related background of using TA as a BCA against AO.

2. Results

We investigated the global transcriptomic shift in *A. ostoyae* (AO) and *T. atroviride* (TA) across three distinct interaction scenarios. Principal component analysis of the data showed that variation was driven by condition, leading to clear grouping of Control (C), Metabolite (M), and Volatile (V)

 doi:10.20944/preprints202604.2000.v1

replicates (Figure 1a; 1b). These distinct clusters suggest that diffusible and airborne cues trigger largely independent transcriptional programs.

Differential expression analysis revealed that the two species responded in an asymmetric fashion. AO showed a massive transcriptional reaction to volatile interaction with 3,234 genes differentially expressed relative to controls (1,658 upregulated, 1,576 downregulated; Figure 1c; Table 1), making it the largest response observed across all comparisons and species. Of these, 2,255 DEGs were unique to volatile conditions and were not differentially expressed under metabolite interaction, demonstrating that AO possesses a qualitatively distinct volatile-specific transcriptional programme. The Metabolite vs. Control comparison yielded 1,965 DEGs (1,126 up, 839 down), and 979 genes responded significantly under both interaction modes. The Volatile vs. Metabolite contrast identified 2,473 additional condition-specific differences, confirming that volatile and metabolite signals engage largely non-overlapping transcriptional circuits in AO (Figure 1e).

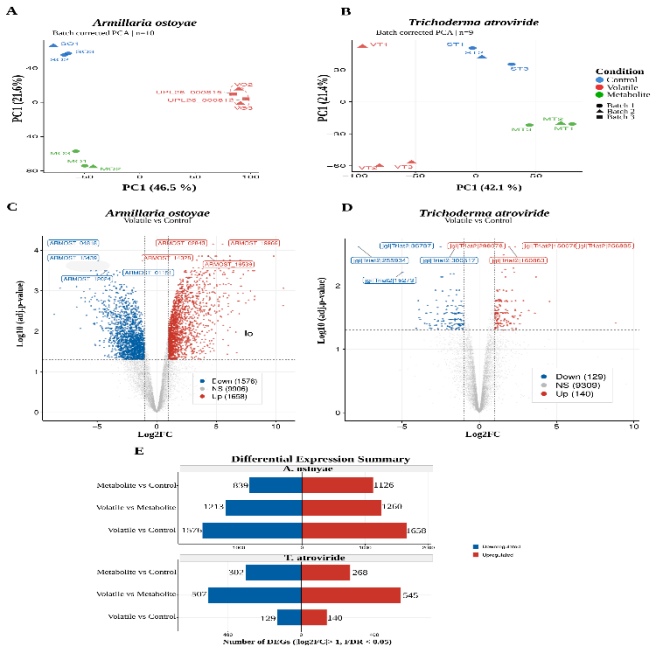

Figure 1. Global transcriptomic reprogramming of *Armillaria ostoyae* and *Trichoderma atroviride* under volatile and metabolite-mediated interactions. (A) Principal component analysis (PCA) of *Armillaria ostoyae* showing separation of control, volatile, and metabolite treatments after batch correction. (B) PCA of *Trichoderma atroviride* highlighting clustering of experimental conditions and temporal variation. (C) Volcano plot of differentially expressed genes (DEGs) in *A. ostoyae* under volatile exposure compared to control. (D) Volcano plot of DEGs in *T. atroviride* under volatile exposure compared to control. (E) Summary of DEG counts across comparisons, illustrating transcriptional responses to volatile and metabolite conditions.

TA responded more selectively: only 269 genes were differentially expressed in V vs. C (140 up, 129 down; Figure 1d), and 570 in M vs. C (268 up, 302 down). Just 68 genes were shared between these two comparisons, yielding 201 volatile-exclusive and 502 metabolite-exclusive DEGs. The Volatile vs. Metabolite contrast nonetheless produced the largest TA DEG set (1,052 genes), indicating that while TA's absolute response to each condition is modest, volatile and metabolite signals produce partially divergent transcriptional states.

 doi:10.20944/preprints202604.2000.v1

Table 1. Differential gene expression across all pairwise contrasts in *Armillaria ostoyae* and *Trichoderma atroviride*.

Species	Comparison	Upregulated	Downregulated	Total
AO	Volatile vs Control	1658	1576	3234
AO	Volatile vs Metabolite	1260	1213	2473
AO	Metabolite vs Control	1126	839	1965
TA	Volatile vs Control	140	129	269
TA	Volatile vs Metabolite	545	507	1052
TA	Metabolite vs Control	268	302	570

2.1. AO Activates Intracellular Detoxification and Suppresses Extracellular Oxygenases in Response to TA

In AO, volatile interaction induced stress-adaptive transcriptional signatures. Upregulated genes were enriched for oxidoreductase activity, glutathione transferase activity, FMN binding, and peroxisomal membrane components (Figure 2a; Table S7a). Together these categories point to activation of intracellular redox buffering, detoxification, and peroxisomal fatty acid metabolism, which are characteristic of fungal responses to cytotoxic volatile exposure. Downregulated genes told an opposing story, dominated by suppression of extracellular secreted proteins, iron ion binding, heme binding, paired-donor oxidoreductase activity acting on molecular oxygen, RNA-directed RNA polymerase complex components, and monooxygenase activity (Figure 2b; Table S7b). The co-enrichment of heme binding, iron binding, and monooxygenase activity defines a large-scale suppression of cytochrome P450-type enzymes, a gene family central to fungal secondary metabolism, xenobiotic detoxification, and lignocellulose degradation. The suppression of RNA-directed RNA polymerase complex components suggests interference with RNA silencing pathways under volatile exposure, an observation that requires further functional investigation. This cytochrome P450 suppression persisted and intensified in the V vs. M comparison, confirming it as a defining feature of volatile-specific signaling rather than a shared response to interaction.

Under metabolite interaction, AO upregulated the same oxidoreductase and FMN-binding categories seen during volatile interaction (oxidoreductase activity, NADPH dehydrogenase activity), indicating shared oxidative reprogramming across interaction modes (Supplementary Figure 1a). However, metabolite contact uniquely downregulated structural constituents of the fungal cell wall and fungal-type cell wall components, a response absent during volatile interaction and potentially reflecting morphological remodelling in response to diffusible secreted compounds in the shared growth medium (Supplementary Figure 1b).

 doi:10.20944/preprints202604.2000.v1

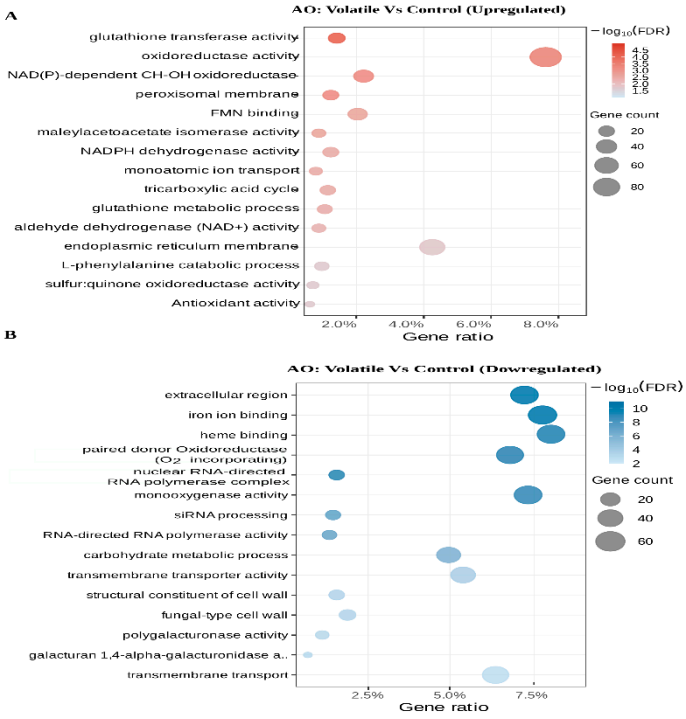

Figure 2. Functional enrichment analysis reveals metabolic and redox-associated responses in *A. ostoyae* under volatile exposure. (A) Gene ontology (GO) enrichment analysis of upregulated genes in *A. ostoyae* under volatile exposure. (B) GO enrichment analysis of downregulated genes in *A. ostoyae* under volatile exposure.

2.2. Volatile Signals from AO Specifically Suppress Non-Ribosomal Peptide Biosynthesis in TA

GO enrichment in TA revealed a biologically compelling pattern centred on secondary metabolism. Under volatile interaction, no statistically significant GO enrichment was detected among either upregulated or downregulated TA genes (minimum BH-adjusted p = 0.114 across all terms tested; Table S9), reflecting the limited number of V vs. C DEGs (269 genes). Nevertheless, a directional signal towards suppression of phosphopantetheine-binding proteins was apparent at a nominal level (3 genes; p.adj = 0.114, supplementary Figure2). Phosphopantetheine is the prosthetic group essential for the activity of non-ribosomal peptide synthetases (NRPS) and polyketide synthases (PKS), enzymes responsible for producing many of the bioactive secondary metabolites for which *Trichoderma* species are known.

Metabolite-mediated interaction produced robust GO enrichment: upregulated TA genes were significantly enriched for oxidoreductase activity, extracellular region proteins, phosphopantetheine binding, amino acid activation for non-ribosomal peptide biosynthesis, and secondary metabolite biosynthetic process (Figure 3a; Table S10a). This activation of NRPS/PKS-associated biosynthetic pathways under direct metabolite contact is further corroborated by the Volatile vs. Metabolite comparison. GO enrichment analysis for genes upregulated in Metabolite showed enrichment of phosphopantetheine binding, extracellular region, amino acid activation for non-ribosomal peptide biosynthesis, and sporulation-related processes are downregulated (Figure 3b; Table S11). Upregulated genes in this comparison were enriched for carboxy-lyase activity and carboxylic acid metabolism, suggesting metabolic rerouting through amino acid catabolism under volatile conditions (Supplementary Figure 2b). Together, these results establish that NRPS/PKS-dependent secondary metabolic pathways are activated by metabolite-mediated contact and relatively suppressed when volatile signals replace direct contact, constituting a mode-dependent regulatory switch in TA secondary metabolism.

 doi:10.20944/preprints202604.2000.v1

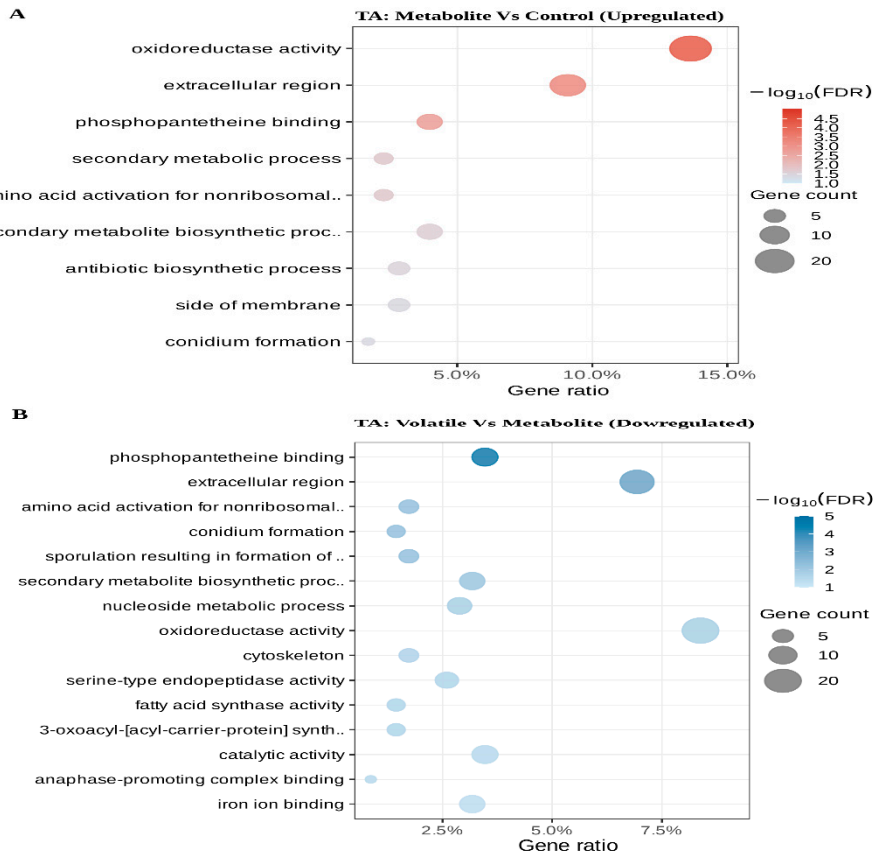

Figure 3. Volatile- and metabolite-induced modulation of secondary metabolism and biosynthetic pathways in *T. atroviride*. (A) GO enrichment analysis of upregulated genes in *Trichoderma atroviride* under metabolite exposure compared to control. (B) GO enrichment analysis of downregulated genes in *T. atroviride* in the volatile versus metabolite comparison.

2.3. Biosynthetic Gene Cluster Analysis Links Terpenoid Activation in AO and Secondary Metabolic Reprogramming in TA to Interaction-Specific Responses

To resolve GO-level signals to specific metabolic loci, we mapped DEGs to antiSMASH-predicted biosynthetic gene clusters (BGCs) and tested each cluster for DEG enrichment using Fisher's exact test with Benjamini–Hochberg correction (Table S22).

In AO, volatile-mediated interaction triggered a reciprocal secondary metabolic switch at the cluster level: upregulated DEGs were significantly enriched in two terpene-related BGCs, Scaffold 1 / Region 4 (terpene; 6/11 cluster genes; FDR = 0.029) and Scaffold 59 / Region 1 (terpene-precursor; 6/10 genes; FDR = 0.029), while downregulated DEGs overlapped significantly with an NRPS-like BGC on Scaffold 24 / Region 1 (9/20 genes; FDR = 0.014) and an NI-siderophore cluster on Scaffold 10 / Region 2 (7/16 genes; FDR = 0.042; Figure 4a). The pattern of terpene cluster activation coinciding with NRPS-like and siderophore cluster suppression was reproduced and strengthened under metabolite-mediated interaction, where four terpene-related BGCs were simultaneously enriched among upregulated DEGs: Scaffold 1 / Region 4 (7/11 genes; FDR = 4.5×10^{-4}), Scaffold 35 / Region 1 (4/4, 100%; FDR = 1.5×10^{-3}), Scaffold 12 / Region 1 (5/9; FDR = 8.0×10^{-3}), and a hybrid T1PKS/terpene-precursor BGC on Scaffold 7 / Region 1 (6/15; FDR = 0.014). The Scaffold 12 / Region 1 cluster is functionally most informative: antiSMASH KnownClusterBlast returned armillyl orsellinate/8α-hydroxy-6-protoilludene (BGC0002445.3) and (−)-cyatha-3,12-diene (BGC0002218.2) as the closest MIBiG references; both bioactive sesquiterpenoids previously characterised from *Armillaria*, directly linking the transcriptional response to compounds known from the AO lineage. The NRPS-like cluster on Scaffold 24 / Region 1 was the most significantly enriched among downregulated DEGs under metabolite interaction (10/20 genes; FDR = 6.1×10^{-6}). The consistent enrichment of multiple

 doi:10.20944/preprints202604.2000.v1

terpene BGCs across both interaction modes indicates that terpenoid biosynthesis is a core component of the AO response to TA, independent of whether interaction is volatile- or metabolite-mediated.

In TA, BGC-level analysis identified condition-dependent regulation of multiple secondary metabolic loci (Figure 4b). Under metabolite-mediated interaction, two T1PKS clusters were strongly activated: Contig 20 / Region 2 (T1PKS; 8/19 cluster genes; FDR = 9.2×10^{-7}) and Contig 21 / Region 1 (T1PKS; 5/16 genes; FDR = 1.3×10^{-3}). An isocyanide cluster on Contig 29 / Region 2 (21 total genes; 4 upregulated; FDR = 0.039) showed more modest activation. The core gene of this isocyanide cluster, jgi|Triat2|48813, encodes a non-ribosomal peptide synthetase fragment with similarity (40.85% identity; e-value: 2×10^{-82}) to NRPS4 of *Bipolaris maydis*; antiSMASH ClusterBlast analysis returned similarity to HC-toxin-like cyclic tetrapeptide clusters from *Alternaria jesenskae* (score 0.73), AM-toxin from *Alternaria alternata* (0.72), and serinocyclin from *Metarhizium robertsii* (0.71), indicating conserved cyclic peptide module architecture within this cluster. Concurrently, two NRPS BGCs were significantly downregulated under metabolite interaction: Contig 27 / Region 8 (19-gene cluster; 7/19 genes; FDR = 4.9×10^{-5}) and Contig 23 / Region 1 (17-gene cluster; 5/17 genes; FDR = 3.2×10^{-3}). The Contig 27 / Region 8 cluster showed clear reciprocal regulation across interaction modes, being upregulated when volatile signals replaced metabolite contact (Volatile vs. Metabolite: 9/19; FDR = 1.5×10^{-5}).

When comparing the volatile and metabolite conditions directly (V vs. M), three clusters were enriched among downregulated genes: the T1PKS cluster on Contig 20 / Region 2 (8/19; FDR = 1.2×10^{-4}), the isocyanide cluster on Contig 29 / Region 2 (8/21; FDR = 1.5×10^{-4}), and an isocyanide-nrp cluster on Contig 26 / Region 5 (5/13; FDR = 5.8×10^{-3}), consistent with their activation by metabolite contact and return to baseline under volatile signaling. Conversely, seven NRPS and isocyanide-type clusters were enriched among upregulated genes in the VvsM comparison, indicating broad relative elevation of these loci under volatile-only versus metabolite-mediated conditions: Contig 27 / Region 8 (NRPS; 9/19; FDR = 1.5×10^{-5}), Contig 22 / Region 2 (NRPS-like; 5/10; FDR = 2.7×10^{-3}), Contig 23 / Region 1 (NRPS; 6/17; FDR = 3.7×10^{-3}), Contig 23 / Region 2 (NRPS; 5/12; FDR = 3.9×10^{-3}), Contig 17 / Region 2 (isocyanide-nrp; 5/16; FDR = 0.014), Contig 29 / Region 1 (isocyanide; 5/17; FDR = 0.016), and Contig 26 / Region 2 (isocyanide-nrp; 5/19; FDR = 0.023). This broader enrichment of NRPS and isocyanide loci in the V vs. M upregulated set establishes that the mode-dependent regulatory switch extends beyond a single locus: T1PKS and select isocyanide clusters are selectively induced by metabolite contact, while multiple NRPS and isocyanide-nrp clusters are relatively elevated under volatile-only signalling. Under volatile vs. control comparison, only the isocyanide-nrp cluster on Contig 26 / Region 5 showed significant enrichment across all DEGs (4/13; FDR = 0.017), with no significant directional enrichment detected in either upregulated or downregulated V vs. C genes alone.

MIBiG annotations provide putative functional context: Contig 21 / Region 1 (T1PKS) shares homology with the aurofusarin biosynthetic cluster, encoding a cytotoxic polyketide red pigment; and Contig 27 / Region 8 (NRPS) shares similarity with the ascochlorin cluster, encoding a terpenoid-polyketide antibiotic relevant to fungal competition. The cluster on Contig 20 / Region 2 (T1PKS) returned similarity to tryptoquialanine-related pathways. These annotations, derived from antiSMASH KnownClusterBlast, should be regarded as putative functional predictions pending experimental validation.

 doi:10.20944/preprints202604.2000.v1

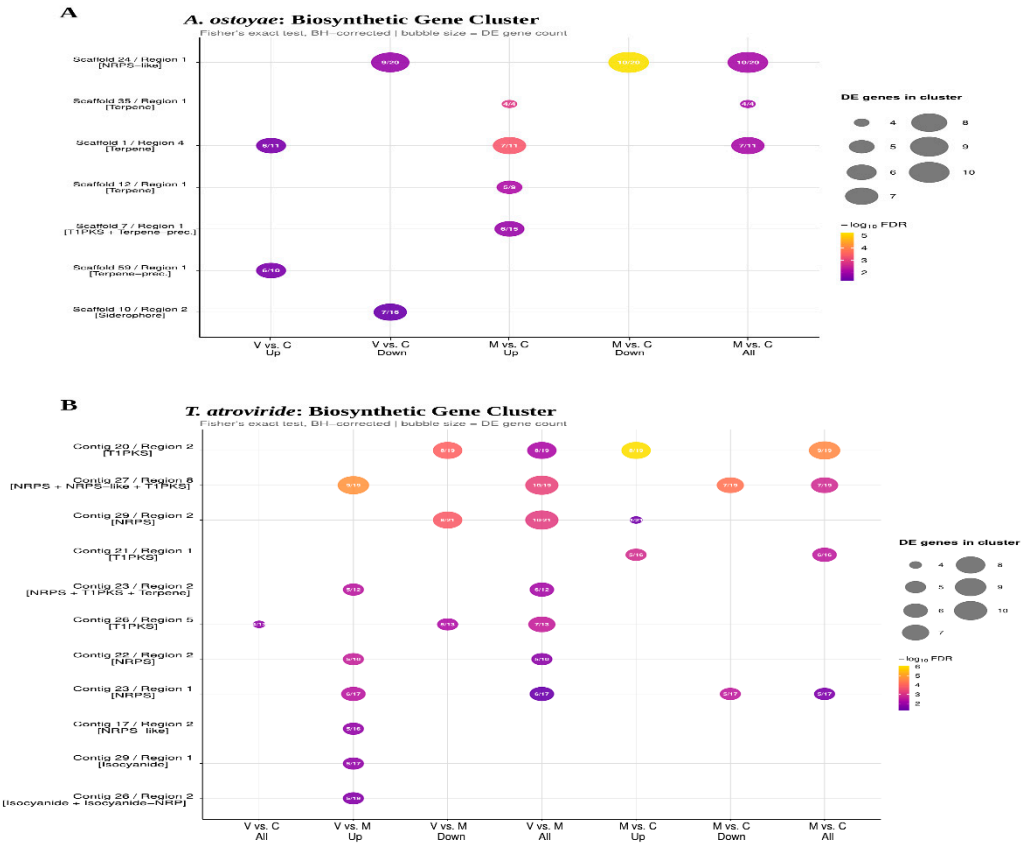

Figure 4. Differential regulation of biosynthetic gene clusters in *A. ostoyae* and *T. atroviride* across interaction conditions. (A) AO BGC enrichment across interaction conditions. (B) TA BGC enrichment across interaction conditions. Bubble size indicates number of DEGs in cluster; colour indicates enrichment direction.

2.4. Co-Culture Suppresses TA C8 Volatile Signals While Triggering Accumulation of an Interaction-Specific Sesquiterpene

VOC profiles were collected from AO, TA, and co-cultured (AT) plates across seven time points spanning from 0 to 62 hours. After removing low-prevalence compounds (>80% zero values), 31 VOCs were retained. PCA and PLS-DA of $\log_2$-transformed abundances both showed clear discrimination among AO, TA, and AT groups throughout the time course, with temporal trajectories visible along secondary ordination axes (Figure 5a; Figure S3). Co-culture produces a chemically distinct headspace environment, one that cannot be explained as a simple mixture of the two monoculture profiles.

Differential VOC analysis using the voom-limma framework revealed that the magnitude of chemical differentiation was greatest during the first 4-8 hours of co-culture, with up to 29 compounds significantly altered between groups at 2 and 4 hours (Figure 5a). This rapid early remodelling of the volatile environment precedes the transcriptomic sampling at 62 hours and likely represents the initial wave of inter-fungal chemical signaling. At 62 hours, the time point most proximate to RNA-seq profiles; 11 VOCs remained significantly different between AO and TA monocultures, and 8 differed between co-culture (AT) and TA monoculture. Crucially, no significant differences between AT and AO monoculture were detected at 62 hours, indicating that the late co-culture volatile environment chemically resembles AO far more closely than TA.

6-Pentyl-2H-pyran-2-one (6-PP), a well-characterised TA secondary metabolite was detectable in TA from the earliest time point (0 h; mean peak area ≈ 45,000 arbitrary units) and increased progressively to peak abundance at 16 h (mean ≈ 674,000), before declining at 32 h (mean ≈ 350,000) and 62 h (mean ≈ 121,000). AO did not produce 6-PP at detectable levels under monoculture conditions, confirming it as a TA-specific volatile (Supplementary Figure 4a). 2-Heptanone, a short-

 doi:10.20944/preprints202604.2000.v1

chain methyl ketone, was absent from TA headspace at early time points (0-8 h) but accumulated substantially from 16 h onwards (mean ≈ 293,000 at 16 h), remaining elevated at 32 h (mean ≈ 23,000) and 62 h (mean ≈ 251,000)(Supplementary Figure 4a); it was likewise undetected in AO monocultures. Because 2-heptanone exceeded the 80% zero-value threshold at early time points, it was excluded from formal differential abundance testing; nevertheless, its raw peak-area dynamics clearly mark it as a late-stage, TA-specific volatile signal. Together, the temporal profiles of these two compounds define distinct windows of TA volatile activity: an early phase (0-8 h) dominated by 6-PP alone, and a late phase (16-62 h) (Supplementary Figure 4a) in which both compounds co-accumulate, consistent with a progression from early-growth-phase 6-PP emission to a more complex and intensifying chemical offensive as TA develops alongside AO.

During interaction (AT), 6-pentyl-2H-pyran-2-one (6-PP) was detectable from the earliest time point (0 h; mean peak area ≈ 1,169 arbitrary units) and increased to higher levels at 16 h (mean ≈ 13,771), before declining at 32 h (mean ≈ 1,169) and increasing again at 62 h (mean ≈ 15,657)(Supplementary Figure 4b). Overall abundance remained substantially lower than in TA monoculture. 2-Heptanone was absent from AT headspace at early time points (0–2 h; mean ≈ 0) but accumulated at 4 h (mean ≈ 4,731) and 8 h (mean ≈ 3,506), before returning to undetectable levels at 16 h and 32 h (mean ≈ 0). A modest increase was observed at 62 h (mean ≈ 6,280)(Supplementary Figure 4b).

The chemical identity of the 8 significantly altered AT vs. TA VOCs was revealing (Table 2; Figure 5b). Six compounds were dramatically reduced in co-culture relative to TA monoculture, three of which, 3-octanone (log_2FC = -15.9; FDR = 2.1×10^{-9}), 3-octanol (log_2FC = -13.6; FDR = 8.9×10^{-7}), and 1-octen-3-ol (log_2FC = -12.5; FDR = 8.2×10^{-9}) are canonical C8 oxygenated fungal volatiles produced by the lipoxygenase-mediated oxidation of linoleic acid. These compounds are among the most studied fungal inter-kingdom and intra-kingdom signaling molecules, reported to suppress spore germination, mediate mycoparasitic recognition, and regulate fungal morphogenesis. Their near-complete elimination from the co-culture headspace is consistent with suppression of TA C8 volatile biosynthesis in the presence of AO, although this could reflect either transcriptional reprogramming in TA in response to AO-emitted cues, enzymatic degradation of C8 compounds by AO, or competitive inhibition in the shared headspace. Two branched alkanes, 3,7-dimethyldecane (log_2FC = -13.2; FDR = 2.1×10^{-9}) and 4,6-dimethyldodecane (log_2FC = -12.1–13.0; FDR < 10^{-8}), were also significantly reduced, indicating a broad suppression of the TA volatile signature rather than inhibition of a single biosynthetic pathway.

Trichloromethane was also significantly reduced in co-culture relative to TA (log_2FC = -1.3; FDR = 3.9×10^{-2}); given its status as a halogenated compound rarely produced biologically, its origin in this experimental system warrants further investigation and it is retained in Table 2 for completeness. The sole compound significantly elevated in co-culture relative to both monocultures was 1-isopropyl-4,7-dimethyl-1,2,3,5,6,8a-hexahydronaphthalene (log_2FC = 9.7 vs. TA, FDR = 3.4×10^{-6}; log_2FC = 9.7 vs. AO, FDR = 3.5×10^{-6}), a cadinane-type sesquiterpene hydrocarbon with a bicyclic skeleton consistent with products of AO terpene BGC activity. This compound is absent from both monocultures under the tested conditions but accumulates specifically during co-culture, mirroring the coordinated upregulation of multiple independent terpene biosynthetic clusters in AO and qualifying it as a strong candidate interaction-induced sesquiterpenoid. At earlier time points, aromatic aldehydes and ketones: benzaldehyde, acetophenone, and 1,4-benzenedicarboxaldehyde, were the most significantly altered compounds in AT vs. AO co-culture (log_2FC ≈ -14 to -15; FDR < 10^{-12}), suggesting that AO also transiently suppresses its own aromatic volatile output at the onset of co-culture.

 doi:10.20944/preprints202604.2000.v1

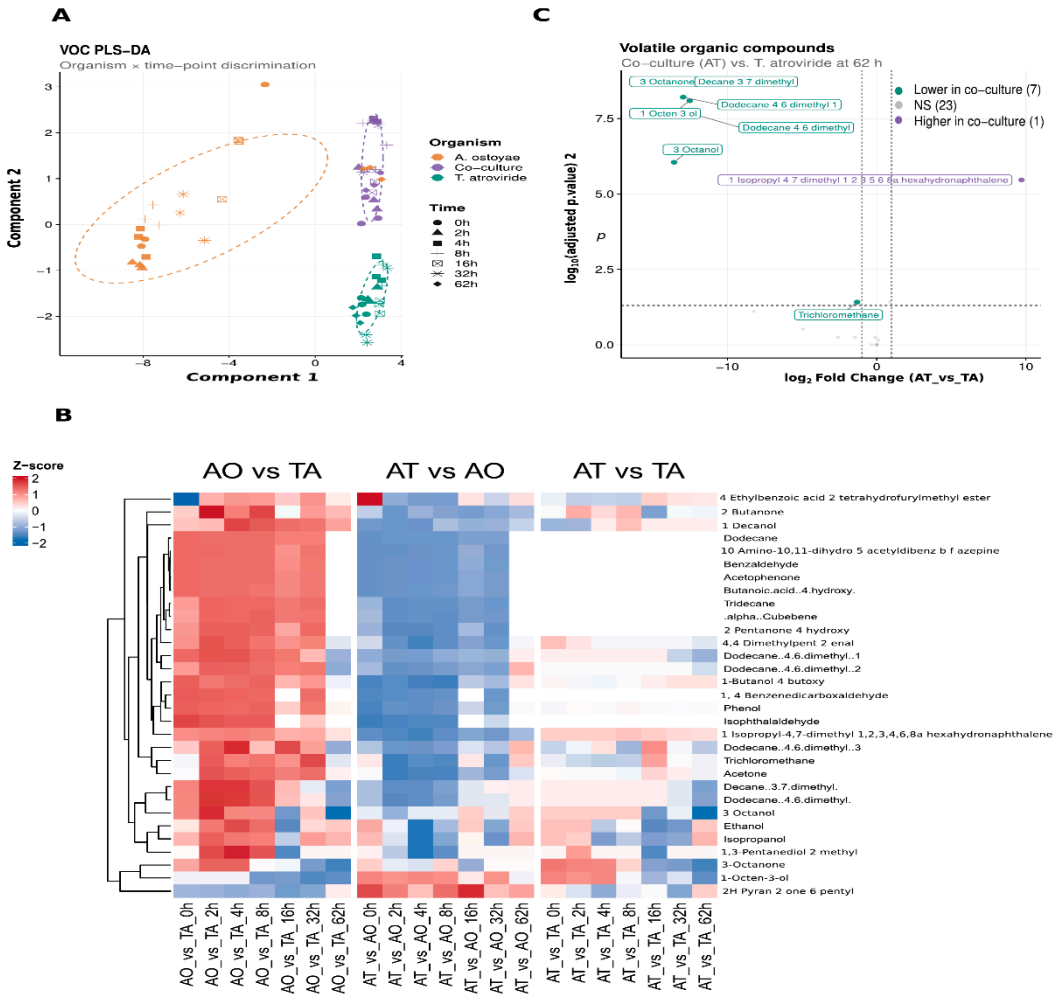

Figure 5. Volatile-mediated interaction dynamics between *A. ostoyae* and *T. atroviride* across time and conditions. (A) Partial least squares discriminant analysis (PLS-DA) of volatile profiles showing separation by organism and time point. (B) Heatmap of volatile organic compound abundance across conditions and time points. (C) Differential analysis of volatile organic compounds in co-culture compared to monoculture conditions (AT vs TA).

Table 2. Volatile organic compounds significantly altered in co-culture AT relative to TA monoculture at 62 hours.

Compound	Class	Log2FC (AT/TA)	FDR
3-Octanone	C8 ketone	-15.9	2.1×10^{-9}
3,7-Dimethyldecane	Branched alkane	-13.2	2.1×10^{-9}
4,6-Dimethyldodecane (isomer 1)	Branched alkane	-13.0	6.2×10^{-9}
4,6-Dimethyldodecane (isomer 2)	Branched alkane	-12.1	2.4×10^{-8}
1-Octen-3-ol	C8 alcohol	-12.5	8.2×10^{-9}
3-Octanol	C8 alcohol	-13.6	8.9×10^{-7}
1-isopropyl-4,7-dimethyl-1,2,3,5,6,8a-hexahydronaphthalene (cadinane-type sesquiterpene)	Sesquiterpene	9.7	3.4×10^{-6}
Trichloromethane	Halogenated	-1.3	3.9×10^{-2}

 doi:10.20944/preprints202604.2000.v1

2.5. Multi-Omics Integration Connects Secondary Metabolic Reprogramming in TA to the Loss of Its C8 Volatile Signature

The evidence from transcriptomics and VOC profiling points towards a coherent mechanism: AO volatile signals remodel secondary metabolism in TA, and this transcriptional reprogramming is reflected in the near-complete disappearance of TA's characteristic bioactive volatile compounds from the co-culture headspace. To test this directly, we integrated the 269 TA DEGs from the Volatile vs. Control comparison with the 8 significantly altered VOCs in AT vs. TA at 62 hours, asking which genes change direction concordantly with each VOC shift.

To quantify the strength and directionality of gene-VOC coupling, we computed concordance scores (gene log_2FC × VOC log_2FC) for all 269 TA DEG × 8 VOC pairs (Table S15, Table S21). By design, the 129 downregulated TA genes produce positive scores against the seven suppressed VOCs (negative × negative), while the 140 upregulated genes produce positive scores against the interaction-elevated sesquiterpene (positive × positive); the informative question is therefore not whether concordance exists but which gene-VOC pairs carry the highest scores and whether specific genes are concordant with multiple C8 compounds simultaneously. The strongest concordance scores were driven by the three C8 oxygenated compounds: 3-octanone (log_2FC = -15.9), 3-octanol (-13.6), and 1-octen-3-ol (-12.5), which together produce the largest magnitude products with highly downregulated TA genes (Figure 6a). Network analysis of the top 1,000 concordant gene-VOC pairs by absolute score revealed a subset of TA genes simultaneously concordant with multiple C8 VOC reductions (Figure 6b), pointing to shared regulatory or biosynthetic nodes upstream of several reduced compounds. Among the most highly connected hub genes were members of the isocyanide BGC on Contig 29 / Region 2, as well as genes associated with T1PKS clusters on Contig 20 / Region 2, consistent with the cluster-level suppression identified by BGC enrichment analysis.

For AO, no VOC differences between co-culture and AO monoculture were detected at 62 hours, precluding a symmetric integration at the primary transcriptomic time point. We note, however, that significant AT vs. AO VOC differences were detected at all earlier time points (0–32 hours), and that the interaction-specific sesquiterpene accumulates specifically in co-culture without being produced by AO monoculture. The 3,234 AO DEGs in V vs. C therefore likely manifest in changes to the early volatile environment and in the de novo production of interaction-specific terpenoids, rather than in alterations to the late steady-state AO volatile profile.

 doi:10.20944/preprints202604.2000.v1

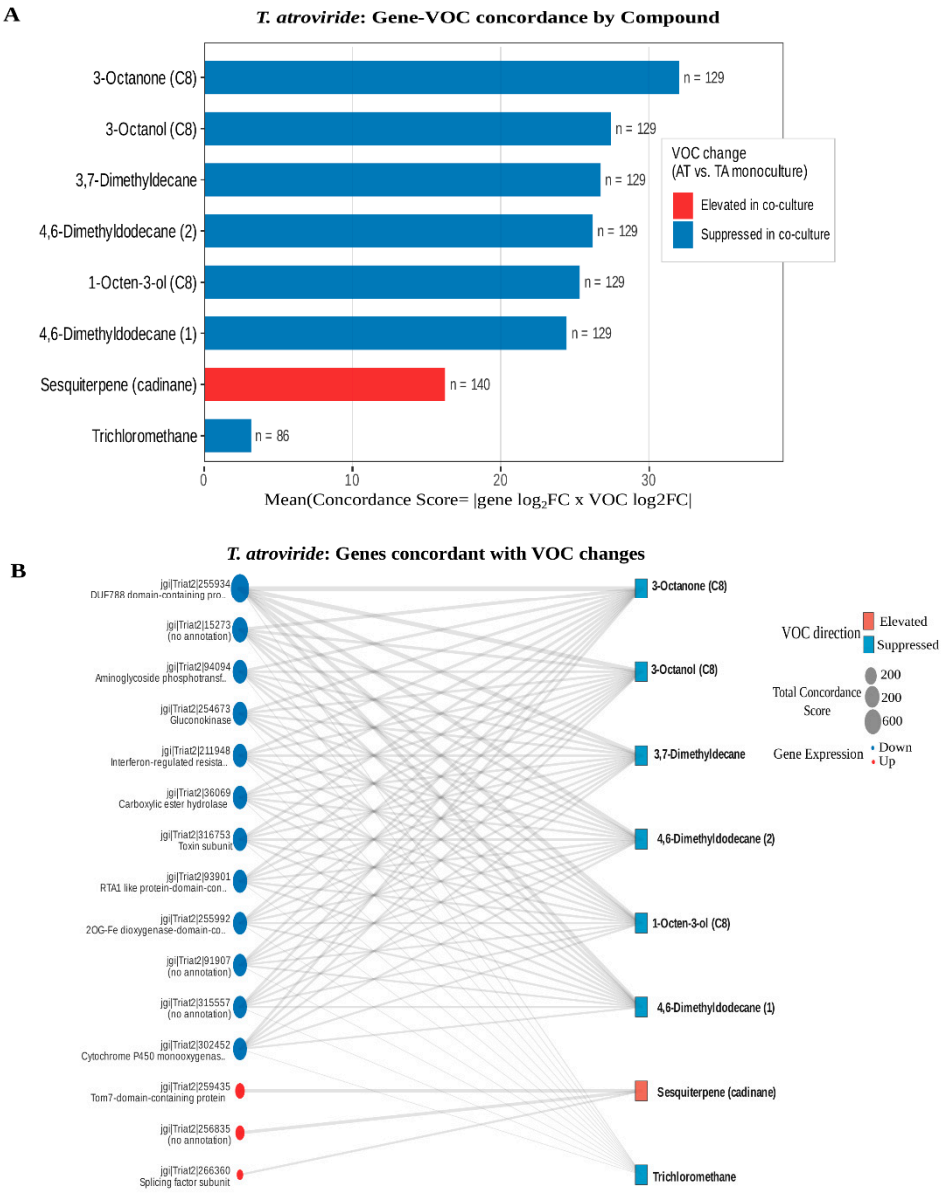

Figure 6. Integration of transcriptomic and volatilomic data reveals gene-VOC concordance in *T. atroviride*. (A) Concordance analysis between gene expression and volatile compound changes in *Trichoderma atroviride*. (B) Network representation of genes associated with variation in volatile compound production.

2.7. Transcriptional Signatures of Volatile-Mediated Sensing Between AO and TA

To identify candidate molecular components involved in volatile-mediated interspecies perception, DEGs from the Volatile vs. Control comparisons were cross-referenced with JGI MycoCosm and PANNZER2 functional annotations.

2.7.1. *Armillaria ostoyae* Activates a Broad Volatile-Sensing Response

Among the 3,234 AO genes differentially expressed under volatile exposure, 32 encoded predicted receptor or ligand-sensing proteins. The most prominent induced class comprised six LysM-domain proteins. Although LysM domains canonically bind chitin oligomers and peptidoglycan at the cell surface, their induction here occurs without direct physical contact, suggesting that volatile cues alone are sufficient to prime non-self-recognition programmes that include cell-wall sensing components, potentially reflecting the activation of a pre-contact defensive state in anticipation of physical encounter. Three CFEM-domain proteins were also strongly induced, together with siderophore iron transporters, indicating activation of iron-competition sensing

 doi:10.20944/preprints202604.2000.v1

pathways. In parallel, two Globin-Coupled Sensor (GCS) domain proteins were highly upregulated, suggesting a potential role for haem-based sensing of reactive or volatile compounds, although their function in fungi remains unresolved.

AO further induced seven G-protein-coupled receptors (GPCRs), including a STE3-like pheromone receptor, raising the possibility that AO perceives TA-derived volatile ligands through pheromone-type receptors, consistent with emerging evidence that fungal GPCRs can detect non-pheromone chemical cues from competing species, while suppressing an RGS-domain regulator, consistent with enhanced G-protein signaling sensitivity. Co-induction of phospholipase C genes supports activation of downstream second-messenger cascades. Several HET-domain proteins were also upregulated, indicating that volatile cues alone are sufficient to trigger pre-contact non-self recognition responses (Figure 7).

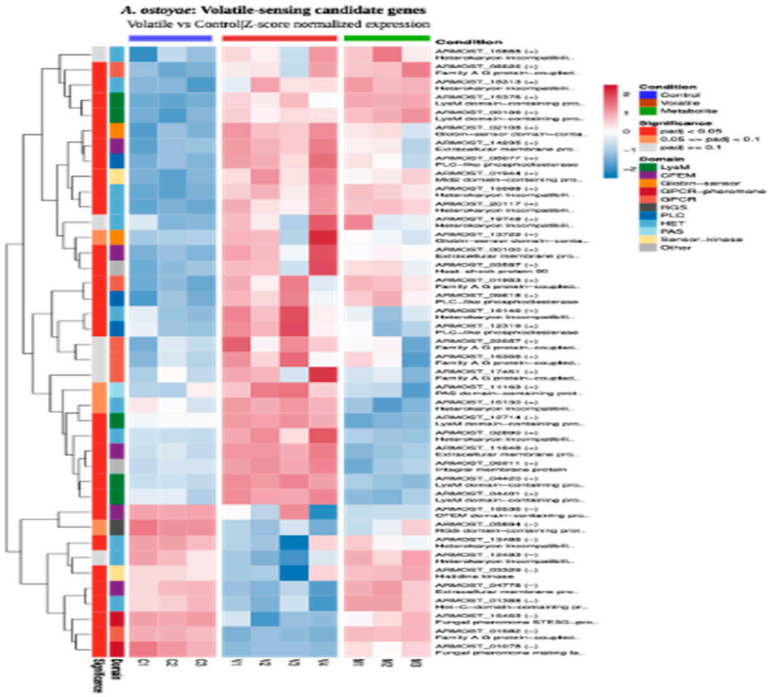

Figure 7. Identification of candidate volatile-sensing genes in *A. ostoyae*.

2.7.2. *Trichoderma atroviride* Mounts a Focused Pre-Contact Sensing Program

TA displayed a smaller but distinct volatile response, with 21 candidate sensory genes identified among 269 DEGs. A Globin-sensor domain protein (logFC = 2.79; padj = 0.25) was among the most strongly nominally induced genes, potentially paralleling the GCS induction observed in AO, though it did not reach statistical significance at the stringent FDR threshold used here.

TA also upregulated the PAS-domain regulator ENVOY, two GPCRs linked to environmental sensing and mycoparasitism, and multiple HET/NACHT-domain proteins, indicating early activation of signal integration and non-self recognition before physical contact. Suppression of a GprK-type GPCR containing an internal RGS domain parallels the GPCR amplification pattern observed in AO. Induction of small secreted proteins further suggests that TA initiates pre-contact extracellular probing upon volatile detection (Figure 8).

 doi:10.20944/preprints202604.2000.v1

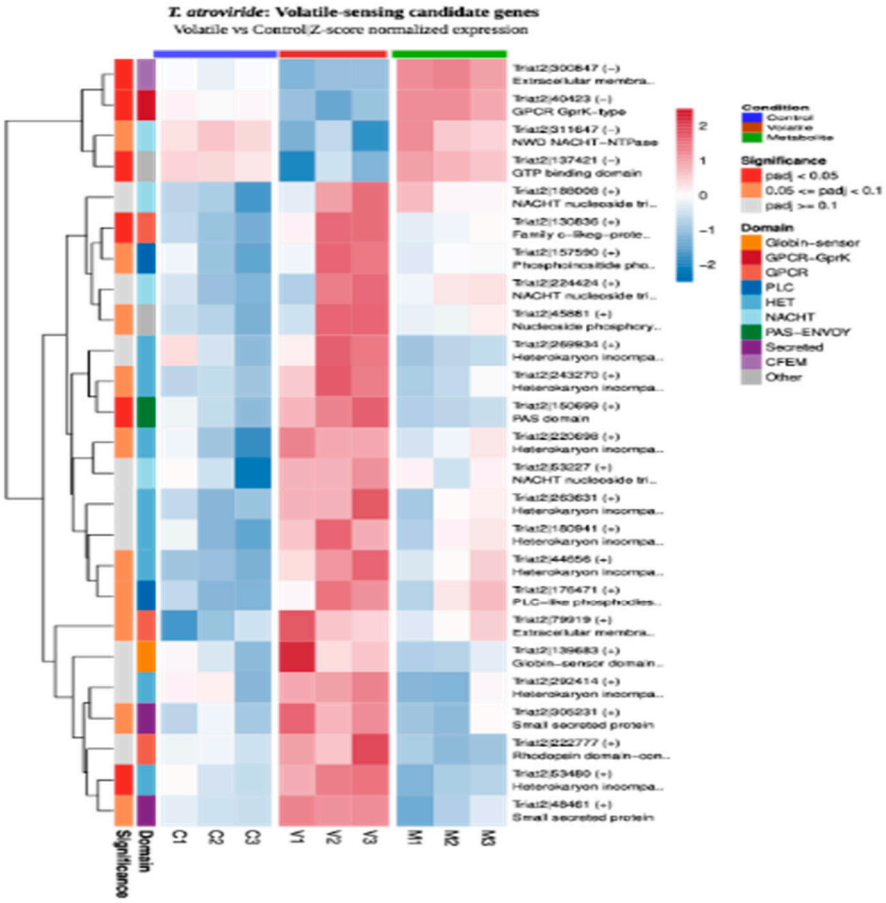

Figure 8. Transcriptional signatures of volatile perception and signaling in *T. atroviride*.

2.7.3. Shared Features of Volatile Sensing in Both Fungi

Despite the asymmetry in response magnitude, AO and TA converged on two common transcriptional features: amplification of GPCR signaling through reduced RGS repression, and activation of downstream signaling components such as phospholipase C. A Globin-sensor domain protein was also nominally elevated in TA (logFC = 2.79), potentially paralleling the significant GCS induction in AO (ARMOST_02108; logFC = 5.20; padj = 2.4×10^{-3}). Together, these patterns suggest that G-protein-mediated signaling may represent a conserved element of fungal volatile-mediated interspecies communication, pending functional validation.

2.8. Quantitative Real-Time PCR (qRT-PCR) Validation

qRT-PCR was performed to validate RNA-seq results using four marker genes previously associated with volatile interaction states, including ARMOST_19697 and ARMOST_01080 (Vol1 markers), and ARMOST_16741 and ARMOST_07302 (Vol2-3 markers). Relative expression levels were calculated across nine biological replicates using actin (ARMOST_03733) as the reference gene. The expression patterns obtained by RT-qPCR were consistent with the transcriptomic data, confirming the expected directionality of regulation for all four markers. However, comparison at the individual sample level revealed variability in response intensity among replicates. Notably, samples 8-2A and 9-2A showed the strongest and most consistent agreement with the Vol2-3 expression profile, characterized by coordinated changes in both downregulated (ARMOST_16741) and upregulated (ARMOST_07302) markers. These expression patterns are indicative of a hypersensitive-like transcriptional state, consistent with the stress-associated responses observed in the RNA-seq dataset under volatile conditions. Based on this strong concordance, samples 8-2A and 9-2A were selected for subsequent transcriptomic analysis, as they most accurately represent the interaction-specific transcriptional response (Figure S8).

 doi:10.20944/preprints202604.2000.v1

3. Discussion

This study was designed to disentangle volatile- and metabolite-mediated interactions between AO and TA, enabling independent assessment of airborne versus diffusible chemical communication. The experimental design successfully resolved distinct interaction states between the two species, as evidenced by the strong clustering of samples by condition in both organisms. This clear condition-specific clustering indicates that both fungi perceive volatile and metabolite signals as biologically distinct stimuli rather than as variations of a single interaction response, supporting the concept that VOC-mediated signaling functions as an independent regulatory layer in fungal interactions. This distinction is particularly important, as it demonstrates that volatile signals alone are sufficient to elicit measurable biological responses in the absence of physical contact. Consistent with previous studies, microbial VOCs have been shown to act as long-distance signaling molecules capable of altering gene expression and behaviour in neighbouring organisms [15]. For example, VOCs produced by *Laccaria bicolor* and *T. atroviride* can alter plant root architecture, while compounds such as 1-octen-3-ol inhibit growth in competing fungi, including *Penicillium* spp., often prior to direct interaction [16]. Together, these findings provide a robust framework for understanding how fungi perceive and respond to competitors in complex environments [17].

The asymmetry in transcriptional responses between the two species is striking. AO exhibited a massive response to volatile exposure, with 3,234 differentially expressed genes (DEGs) with enrichment for oxidative stress-related processes including antioxidant activity, glutathione metabolism and oxidoreductase functions (Figure 3a), indicative of redox imbalance and activation of cellular detoxification mechanisms. Consistent with this, nine apoptosis-related genes were upregulated, including AIF1 (ARMOST_01402; $\log_2$FC=2.4), a Bax Inhibitor family protein (ARMOST_09409; $\log_2$FC = 2.6), and Amid-like NADH oxidoreductases (ARMOST_18535/18537; $\log_2$FC = 4.8-5.2; Table S1; Figure S5), suggesting that volatile-induced stress reaches thresholds sufficient to engage programmed cell death pathways. A comparable transcriptional signature involving metacaspases and apoptosis-inducing factors has been reported during direct AO-TA interaction, where oxidative stress and toxic metabolite exposure drive similar apoptotic activation [11]. These findings position apoptosis-related pathways as integral components of a broader stress adaptation strategy tightly coupled to redox homeostasis [19–21]. The haploid status of the AO isolate may further amplify this response: without the allelic buffering present in diploid or heterokaryotic fungi, stress-responsive loci are expressed without regulatory dampening, rendering the isolate an unusually sensitive reporter of chemical interaction signals. Additionally, the evolutionary distance between AO (basidiomycete root pathogen) and TA (ascomycete mycoparasite) likely precludes refined counter-recognition mechanisms, favoring a broad generalized alarm response to a phylogenetically distant chemical threat [18].

The scale of this response is further supported by the 2,255 AO genes that were uniquely responsive to volatile exposure and Volatile vs. Metabolite comparison revealed additionally 2,473 differences confirming largely non-overlapping transcripts for airborne and diffusible signals (Figure S1; Figure 2b). This supports the existence of a dedicated volatile-specific regulatory program, consistent with studies in other fungal systems demonstrating that VOCs modulate gene expression, thereby affecting protein synthesis and enzyme activity through distinct signalling pathways [22–24]. For instance, *Trichoderma*-derived volatiles inhibit protein synthesis in *Serpula lacrymans* in the absence of physical contact [25], and stress-induced VOC changes in *Saccharomyces cerevisiae* associated with large-scale transcriptional reprogramming [24].

The downregulated gene set in AO under volatile exposure was enriched for monooxygenase activity, heme binding, and iron ion binding (Figure 3b), indicating suppression of cytochrome P450-dependent metabolism and a shift away from extracellular oxidative transformation pathways of xenobiotics [26–31]. Notably, concurrent downregulation of 14 RNA-directed RNA polymerase (RdRP) complex genes (FDR = 8.1×10^{-10}) suggests interference with RNAi-related defense pathways, possibly reflecting metabolic resource reallocation toward acute stress responses during chemical

 doi:10.20944/preprints202604.2000.v1

challenge; the functional significance of RdRP suppression during volatile interactions warrants further investigation.

A likely driver of the observed AO response is exposure to TA-derived volatiles, particularly 6-pentyl-α-pyrone (6-PP) and 2-heptanone [32]. 6-PP, a dominant polyketide VOC of *Trichoderma spp*., [33], disrupts plasma membrane organization and cell wall integrity [34,35], consistent with the transcriptional changes observed in AO in genes encoding hydrophobins, chitin synthases, β-glucans, mannoproteins, and fatty acid desaturases (Figure S6). Indicating active restructuring of the cell surface and membrane composition in response to chemical stress. Cell wall remodeling is a well-established fungal adaptation that modulates structural integrity and permeability under stress conditions [36–38]. Additionally, 6-PP promotes ROS accumulation [34], which can overwhelm antioxidant defenses and disrupt DNA replication and cell cycle progression (Figure S7) [26,40]. 2-Heptanone, while detected during interaction and reported to exert antifungal activity against several plant pathogens [39,41], has an incompletely characterized mode of action and likely contributes to AO stress responses in combination with other volatile compounds rather than through a singular mechanism.

By contrast, TA exhibited a far more restricted response of only 269 DEGs, with enrichment pointing toward secondary metabolite biosynthesis and interaction-related functions (Figs. 3c, 3d), consistent with the targeted molecular arsenal TA deploys during competitive interactions, including cell wall-degrading enzymes and secondary metabolite pathways [11]. This asymmetry reflects fundamentally distinct adaptive strategies: AO engages in broad, stress-associated defensive reprogramming, while TA adopts a focused antagonistic program based on specialized interaction mechanisms [21].

Metabolite-mediated interaction in TA strongly activated genes encoding phosphopantetheine-binding enzymes, the essential cofactors for non-ribosomal peptide synthetases (NRPS) and polyketide synthases (PKS) [42,43]. Conversely, when volatile signals replaced metabolite contact (V vs. M), PKS/NRPS-associated functions were relatively suppressed while carboxy-lyase and carboxylic acid metabolism pathways became elevated. This reciprocal regulation constitutes a clear mode-dependent switch in TA secondary metabolism, consistent with the high environmental responsiveness of Trichoderma biosynthetic gene clusters (BGCs) [44]. The polyketide 6-PP exemplifies this regulation: its PKS-dependent biosynthesis is directly linked to antifungal activity, and disruption of this cluster reduces competitive fitness [45,46].

BGC-level analysis revealed a structured reorganization of secondary metabolism in both organisms under interaction conditions. In AO, upregulated terpene clusters and repression of an NRPS-like cluster indicate coordinated modulation of individual biosynthetic loci rather than diffuse pathway-level changes. Enrichment of clusters related to protoilludene-derived, melleolide-type pathways is characteristic of *Armillaria* sesquiterpenoid metabolism [47,48]. More broadly, fungal terpenoid biosynthesis relies on terpene cyclases and tailoring enzymes to generate structurally diverse metabolites [49]. In TA, two T1PKS clusters and an isocyanide cluster (Contig 29/Region 2) were strongly activated under metabolite contact, while multiple NRPS and isocyanide-nrp clusters showed higher expression under volatile-only conditions; most prominently Contig 27/Region 8, with six additional loci sharing the same directional pattern in the V vs. M comparison. This reciprocal, locus-specific regulation across multiple BGC classes defines a clear interaction-dependent metabolic reorganization, consistent with the modular architecture of fungal secondary metabolism in which BGCs function as independently regulated genetic units [50]. The interaction-dependent activation of specific clusters is further consistent with the well-documented transcriptional silencing of BGCs under standard conditions and their induction by environmental or interspecies stimuli [50–52].

The volatile profiles provide chemical-level support for these transcriptional findings. Pronounced divergence in the shared volatilome within the first 4-8 hours of co-culture indicates that volatile-mediated signaling represents an early interaction layer, preceding the transcriptional responses observed at later time points [53]. A dominant feature of this interaction was near-complete

 doi:10.20944/preprints202604.2000.v1

suppression of TA-associated C8 oxygenated compounds: 1-octen-3-ol, 3-octanone, and 3-octanol in co-culture, indicating disruption of TA's primary volatile signaling system. These oxylipin-like compounds, derived from polyunsaturated fatty acid oxidation, regulate fungal development and interspecific communication [54,55], and their loss alongside additional compound classes suggests a broad suppression of TA volatile output rather than inhibition of a single biosynthetic pathway. Temporal analysis revealed a structured progression of TA volatile activity: 6-PP peaked at 16 hours before declining, consistent with its growth-phase-dependent accumulation [32], while 2-heptanone emerged after 16 hours and remained elevated through 62 hours, indicating distinct temporal phases of volatile emission.

In contrast to the suppression of TA-associated signals, co-culture was characterized by accumulation of a cadinane-type sesquiterpene absent from both monocultures, providing a direct chemical correlate to terpene BGC activation in AO. Cadinane-type compounds, such as δ-cadinene, are produced via conserved terpene synthase pathways and many fungal sesquiterpenoids exhibit antimicrobial or cytotoxic activities [56,57], supporting their functional relevance in competitive environments.

Multi-omics concordance analysis further confirmed tight coupling between gene regulation and volatile output. C8 oxygenated compounds showed the highest concordance scores (log_2FC: 1-octen-3-ol = -12.5; 3-octanone = -15.9; 3-octanol = -13.6), and network analysis identified genes concordant with multiple C8 VOC reductions, including biosynthetic genes associated with isocyanide and T1PKS clusters. This gene–metabolite coupling supports a system-wide suppression of TA's volatile-mediated communication, consistent with multi-omics studies demonstrating tight coordination between transcriptional regulation and metabolite accumulation [58,59]. Similar coordinated reprogramming has been observed in fungal–bacterial interactions, such as between *T. asperellum* and *Bacillus subtilis* [60].

Finally, volatile exposure alone was sufficient to engage defined sensory and signaling pathways in both species. In AO, induction of LysM- and CFEM-domain proteins alongside GPCR-associated components indicates activation of environmental sensing and iron acquisition-related signaling [61,62], with concurrent modulation of RGS activity supporting engagement of canonical stress-adaptive signal transduction cascades [63]. In TA, a more focused sensing response involving GPCRs, the PAS-domain regulator ENVOY, and HET/NACHT-associated proteins is consistent with targeted environmental signal integration [64]. Notably, a Globin-sensor domain protein was significantly induced in AO (ARMOST_02108; log_2FC = 5.20), with a nominally elevated orthologue in TA, suggesting a potential role for haem-associated systems in sensing redox and volatile signals [62]. Together, these findings support a model of pre-contact chemical perception mediated by conserved GPCR-dependent signaling architectures acting in concert with species-specific sensing modules [22].

4. Materials and Methods

4.1. Dual-Culture Face-Off Between Trichoderma atroviride and Armillaria ostoyae Colonies

Armillaria ostoyae SZMC 23085 and *Trichoderma atroviride* SZMC 24276 were cultured on potato dextrose agar (PDA) as described in [11]. Three experimental conditions were used: axenic controls (C), side-by-side colonies (M) permitting diffusible metabolite exchange, and paired-plated cultures (V) permitting only airborne volatile communication (Figure S9).

Control (C) and Metabolite (M) samples were harvested at 53 h post-inoculation (data previously published in [11]. For the Volatile (V) interaction, fungal colonies were co-cultivated in a closed, shared-airspace arrangement and harvested after 62 h. Due to an outlier identified in the initial volatile sample set, three additional volatile replicates were grown and sequenced in a separate batch to ensure statistical power. In total, ten *A. ostoyae* samples (3 C, 3 M, 4 V) and nine *T. atroviride* samples (3 per condition) were analyzed.

 doi:10.20944/preprints202604.2000.v1

4.2. Transcriptomic Analysis

Raw reads were processed with FastP v1.3.2 for adapter trimming and quality filtering, and aligned to species-specific reference genomes (*Armillaria ostoyae* in-house assembly, Sipos et al. 2017; and *Trichoderma atroviride* v2.0, JGI MycoCosm) using STAR v2.7.11b in two-pass mode with default parameters. Gene-level expression was quantified as expected counts using RSEM v1.3 with default parameters. All downstream analyses were performed in R v4.3.3. Raw count matrices were imported for *A. ostoyae* (AO) and *T. atroviride* (TA), rounded to integers, and library sizes normalised using the trimmed mean of M-values (TMM) method as implemented in edgeR v4.0.16. Low-expression genes were removed using filterByExpr with default parameters and condition-based grouping, retaining 13,140 AO and 9,578 TA genes.

Transcriptomic libraries were generated across three batches. Sample quality was assessed in two stages. First, PCA of TMM-normalized log-CPM values was used to automatically flag samples deviating more than three standard deviations from the mean along PC1 or PC2. Second, additional samples were excluded following visual inspection of multidimensional scaling (MDS) plots of batch-corrected expression values, which revealed samples with batch-driven separation inconsistent with their assigned condition. This led to the exclusion of two *A. ostoyae* samples (VO1, UPL26_000814) originating from batches 1 and 3. To account for technical noise, batch was included as a covariate in the voom-limma design matrix. For visualization purposes only, batch effects were removed from log-CPM values using removeBatchEffect (limma v3.66), with the experimental condition included in the design matrix to preserve biological variation. These corrected values were used solely for PCA and heatmaps and were excluded from the formal statistical modeling. Differential expression was performed using the voom-limma pipeline on the retained samples. Pairwise contrasts were defined between all three conditions for each species independently. Genes were considered differentially expressed at a Benjamini–Hochberg adjusted p-value < 0.05 and $|\log_2 FC| \geq 1$.

4.3. Gene Ontology and Biosynthetic Gene Cluster Enrichment Analysis

Gene Ontology (GO) annotation was done using PANNZER2 on 06 April, 2026 for both AO and TA. GO overrepresentation analysis was performed independently for upregulated and downregulated DEG sets in each contrast using clusterProfiler v4.10.0. Biosynthetic gene cluster (BGC) annotations were obtained from antiSMASH analyses of the AO and TA genomes. For each pairwise contrast and direction (upregulated, downregulated, combined), enrichment of DEGs within each annotated BGC was assessed using a one-sided Fisher's exact test. P-values were corrected for multiple testing using the Benjamini-Hochberg method across all BGCs tested within each contrast. BGCs with a BH-adjusted p-value < 0.05 were considered significantly enriched.

4.4. Volatile Organic Compound Profiling

Headspace volatile organic compound (VOC) profiles were collected from AO, TA, and co-cultured (AT) plates at seven time points (0, 2, 4, 8, 16, 32, and 62 hours). VOCs were extracted using HS-SPME with a 50/30 µm DVB/CAR/PDMS fiber (Merck, Hungary). Fiber extraction was performed at 40 °C for 10 min following a 10-min preconditioning at 260 °C. Samples were analyzed using a Shimadzu QP 2020 GCMS equipped with an AOC 6000 autosampler. Desorption occurred at 250 °C for 2 min in splitless mode using a TraceGOLD™ TG-Wax-MS column (60 m × 0.25 mm × 0.25 µm). The oven program started at 40 °C (3.5 min hold), increased at 4 °C/min to 220 °C, and held for 5 min. The MS was operated in EI mode (70 eV) with a scan range of 33-550 Da.

Compounds were identified by comparison against the NIST 5V mass spectral library with a minimum match score threshold of 80% and quantified as peak area values. Compounds with more than 80% zero values across all samples were excluded, retaining 31 VOCs. Peak areas were $\log_2$-transformed (after adding a pseudo count of 1) to stabilize variance. Principal component analysis (PCA) was performed on the scaled and centered matrix using 'prcomp' in R. Partial Least Squares Discriminant Analysis (PLS-DA) was performed using mixOmics v6.26.0 with three components and

 doi:10.20944/preprints202604.2000.v1

a random seed of 42. Differential abundance was assessed at each time point using the voom–limma framework. VOCs were considered significantly altered at BH-adjusted p-value < 0.05 and $|\log_2 FC| \geq 1$.

4.5. Multi-Omics Integration

To identify candidate genes whose transcriptional changes are concordant with VOC alterations in co-culture, DEGs from the TA Volatile vs. Control comparison were integrated with significantly altered VOCs in the AT vs. TA comparison at 62 hours. For each gene-VOC pair, directional concordance was defined as agreement in the sign of the gene's $\log_2 FC$ (Volatile vs. Control) and the VOC's $\log_2 FC$ (AT vs. TA): a positive score indicates that a gene upregulated under volatile interaction is paired with a VOC elevated in co-culture, and vice versa. A concordance score was computed as the product of the two $\log_2 FC$ values (score = gene_logFC × voc_logFC), such that positive values indicate concordance and larger absolute values indicate stronger co-directional responses. The top 1,000 concordant gene-VOC pairs ranked by absolute concordance score were retained. DEGs within this set were cross-referenced against antiSMASH BGC [14] annotations to identify cluster membership. Gene-VOC association networks were constructed using igraph v2.0.3 and visualised using ggraph v2.2.1.

4.6. Quantitative Real-Time PCR (qRT-PCR) Validation

To validate transcriptomic data, qRT-PCR was performed using a Bio-Rad CFX96 Real-Time PCR Detection System. First-strand cDNA was synthesized from total RNA using the SuperScript IV First-Strand Synthesis System (Invitrogen) with random hexamer primers, with the synthesis step extended to 30 seconds to improve yield from low-concentration templates. Amplification reactions were carried out using PowerTrack SYBR Green Master Mix (Applied Biosystems) under the following cycling conditions: initial denaturation at 95 °C for 3 min, followed by 40 cycles of 95 °C for 5 s, 60 °C for 30 s, and 72 °C for 30 s. Primer sequences are listed in Supplementary Table S24.

A total of nine biological replicates obtained from independent face-off experiments were analyzed. Gene expression was assessed using four marker genes previously characterized under different volatile interaction conditions, including ARMOST_19697 and ARMOST_01080 (Vol1-associated markers), as well as ARMOST_16741 and ARMOST_07302 (Vol2 and Vol3-associated markers). Relative gene expression levels were calculated using the 2^−ΔΔCt method [13], with actin (ARMOST_03733) used as the internal reference gene for normalization.

4.7. Data Visualisation and Statistical Software

All analyses were performed in R v4.3.3 and ggplot2 was used for plotting

4.8. Use of Generative Artificial Intelligence (GenAI)

Generative artificial intelligence tools were used to assist in the organization, drafting, and refinement of the manuscript. All scientific analyses, results, and final interpretations were performed, critically evaluated, and validated by the authors.

5. Conclusions

Volatile and metabolite signals represent distinct drivers of fungal interaction dynamics between *Armillaria ostoyae* and *Trichoderma atroviride*. Airborne signals alone trigger extensive transcriptional reprogramming in AO, characterized by redox imbalance and detoxification, while TA exhibits targeted regulation of secondary metabolism. The coupling between gene expression and volatile output, including suppression of C8 compounds and mode-dependent regulation of polyketide and isocyanide biosynthetic clusters, demonstrates how chemical signalling is encoded at the transcriptional level. Concurrent activation of terpene biosynthesis and interaction-specific sesquiterpenes further reflects a coordinated metabolic shift during competition. These findings

 doi:10.20944/preprints202604.2000.v1

highlight volatile signaling as a key factor in early interaction outcomes and support its potential exploitation in *Trichoderma*-based biocontrol strategies against *Armillaria*.

Supplementary Materials: The following supporting information can be downloaded at the website of this paper posted on Preprints.org, Figure S1a: AO_MvsC_GO_down; Figure S1b: AO_MvsC_GO_up; Figure S2a: TA_VvsC_GO_down; Figure S2b: TA_VvsM_GO_up; Figure S3: VOC_PCA; Figure S4: Volatile emission dynamics (TA vs AT); Figure S5: AO_cellwall; Figure S6: AO_cellcycle; Figure S7: AO_apoptosis_lineplot; Figure S8: qPCR; Figure S9: experimental setup for volatile interaction; Table S1: AO_VvsC_DEA; Table S2: AO_VvsM_DEA; Table S3: AO_MvsC_DEA; Table S4: TA_VvsC_DEA; Table S5: TA_VvsM_DEA; Table S6: TA_MvsC_DEA; Table S7a: AO_VvsC_GO_up; Table S7b: AO_VvsC_GO_down; Table S8a: AO_MvsC_GO_up; Table S8b: AO_MvsC_GO_down; Table S9: TA_VvsC_GO_down; Table S10a: TA_MvsC_GO_up; Table S10b: TA_MvsC_GO_down; Table S11: TA_VvsM_GO_down; Table S12: AO_BGC_enrichment; Table S13: TA_BGC_enrichment; Table S14: VOC_differential_analysis; Table S15: TA_gene_VOC_concordance; Table S16: DEG_count_summary; Table S17: AO_PCA_coordinates; Table S18: TA_PCA_coordinates; Table S19: VOC_PLSDA_scores; Table S20: VOC_timecourse_logFC; Table S21: TA_geneVOC_score_matrix; Table S22: BGC_enrichment_all; Table S23: TA_VvsM_GO_up; Table S24: Primers; Table S25a: AO_VvsM_GO_up; Table S25b: AO_VvsM_GO_down.

Author Contributions: Conceptualization, G.S. and L.K.; methodology, O.L., S.C., O.K., and An.Sz; software, S.C.; An.Sz.; validation, At.Sz., S.K., G.N., and B.I.; formal analysis, NT.L-E., O.L. and S.C.; investigation, O.L.; O.K., B.I., and S.C.; resources, Á.B. and YR.D.; data curation, S.C.; O.L.; writing—original draft preparation, G.S.; O.L., and S.C.; writing—review and editing, NT.L-E.; L.K., Cs.V., and G.S.; visualization, O.L.; At. Sz., and S.C. ; supervision, G.S., K.L., and Cs.V.; project administration, G.S.; L.K., Cs.V.; funding acquisition, G.S.; L.K.; YR.D., and Cs.V. All authors have read and agreed to the published version of the manuscript.

Funding: This research was funded by the project 2022-1.2.6-TÉT-IPARI-TR-2022-00009, implemented by the Ministry of Culture and Innovation of Hungary from the National Research, Development and Innovation Fund, financed under the 2024-1.2.11-TÉT-IPARI-TR funding scheme. G.S. also acknowledges funding from the grant EGF/388/2025 provided by the Ministry of Agriculture.

Institutional Review Board Statement: Not applicable.

Informed Consent Statement: Not applicable.

Data Availability Statement: We encourage all authors of articles published in MDPI journals to share their research data. In this section, please provide details regarding where data supporting reported results can be found, including links to publicly archived datasets analyzed or generated during the study. Where no new data were created, or where data is unavailable due to privacy or ethical restrictions, a statement is still required. Suggested Data Availability Statements are available in section "MDPI Research Data Policies" at https://www.mdpi.com/ethics.

Acknowledgments: The research was performed in collaboration with the Genomics and Bioinformatics Core Facility at the Szentágothai Research Centre of the University of Pécs.

Conflicts of Interest: All authors declare that there is no conflict of interest.

References

1. Baumgartner, K., Coetzee, M. P. A., & Hoffmeister, D. (2011). Secrets of the subterranean pathosystem of Armillaria. Molecular Plant Pathology, 12(6), 515–534. https://doi.org/10.1111/j.1364-3703.2010.00693.x
2. Kedves, O., Shahab, D., Champramary, S., Chen, L., Indic, B., Bóka, B., Nagy, V. D., Vágvölgyi, C., Kredics, L., & Sipos, G. (2021). Epidemiology, biotic interactions and biological control of armillarioids in the Northern hemisphere. Pathogens, 10(1), 76. https://doi.org/10.3390/pathogens10010076
3. Bendel, M., Kienast, F., Bugmann, H., & Rigling, D. (2006). Incidence and distribution of Heterobasidion and Armillaria and their influence on canopy gap formation in unmanaged mountain pine forests in the Swiss Alps. European Journal of Plant Pathology, 116(2), 85–93. https://doi.org/10.1007/s10658-006-9028-1

 doi:10.20944/preprints202604.2000.v1

4. Sipos, G., Anderson, J. B., & Nagy, L. G. (2018). Armillaria. Current Biology, 28(7), R297–R298. https://doi.org/10.1016/j.cub.2018.01.026
5. Desprez-Loustau, M., Marçais, B., Nageleisen, L., Piou, D., & Vannini, A. (2006). Interactive effects of drought and pathogens in forest trees. Annals of Forest Science, 63(6), 597–612. https://doi.org/10.1051/forest:2006040
6. Yafetto, L. (2018). The structure of mycelial cords and rhizomorphs of fungi: A minireview. Mycosphere, 9(5), 984–998. https://doi.org/10.5943/mycosphere/9/5/3
7. McLaughlin, M. S., Roy, M., Abbasi, P. A., Carisse, O., Yurgel, S. N., & Ali, S. (2023). Why do we need alternative methods for fungal disease management in plants? Plants, 12(22), 3822. https://doi.org/10.3390/plants12223822
8. Knudsen, G. R., & Dandurand, L. C. (2014). Ecological complexity and the success of fungal biological control agents. Advances in Agriculture, 2014, 1–11. https://doi.org/10.1155/2014/542703
9. Seidl, V., Song, L., Lindquist, E., Gruber, S., Koptchinskiy, A., Zeilinger, S., Schmoll, M., Martínez, P., Sun, J., Grigoriev, I., Herrera-Estrella, A., Baker, S. E., & Kubicek, C. P. (2009). Transcriptomic response of the mycoparasitic fungus Trichoderma atroviride to the presence of a fungal prey. BMC Genomics, 10(1), 567. https://doi.org/10.1186/1471-2164-10-567
10. Harman, G. E., Howell, C. R., Viterbo, A., Chet, I., & Lorito, M. (2004). Trichoderma species — opportunistic, avirulent plant symbionts. Nature Reviews Microbiology, 2(1), 43–56. https://doi.org/10.1038/nrmicro797
11. Chen, L., Champramary, S., Sahu, N., Indic, B., Szűcs, A., Nagy, G., Maróti, G., Pap, B., Languar, O., Vágvölgyi, C., Nagy, L. G., Kredics, L., & Sipos, G. (2023). Dual RNA-Seq Profiling Unveils Mycoparasitic Activities of Trichoderma atroviride against Haploid Armillaria ostoyae in Antagonistic Interaction Assays. Microbiology Spectrum, 11(3), e0462622. https://doi.org/10.1128/spectrum.04626-22
12. Reithner, B., Ibarra-Laclette, E., Mach, R. L., & Herrera-Estrella, A. (2011). Identification of Mycoparasitism-Related Genes in Trichoderma atroviride. Applied and Environmental Microbiology, 77(13), 4361–4370. https://doi.org/10.1128/aem.00129-11
13. Livak, K. J., & Schmittgen, T. D. (2001). Analysis of relative gene expression data using Real-Time Quantitative PCR a nd the 2−ΔΔCT method. Methods, 25(4), 402–408. https://doi.org/10.1006/meth.2001.1262
14. Blin, K., Shaw, S., Augustijn, H. E., Reitz, Z. L., Biermann, F., Alanjary, M., Fetter, A., Terlouw, B. R., Metcalf, W. W., Helfrich, E. J. N., Van Wezel, G. P., Medema, M. H., & Weber, T. (2023). antiSMASH 7.0: new and improved predictions for detection, regulation, chemical structures and visualisation. Nucleic Acids Research, 51(W1), W46–W50. https://doi.org/10.1093/nar/gkad344
15. Lee, S., Hung, R., & Bennett, J. W. (2024). An overview of fungal Volatile Organic Compounds (VOCs). In The mycota (pp. 83–111). https://doi.org/10.1007/978-3-031-41648-4_4
16. Werner, S., Polle, A., & Brinkmann, N. (2016). Belowground communication: impacts of volatile organic compounds (VOCs) from soil fungi on other soil-inhabiting organisms. Applied Microbiology and Biotechnology, 100(20), 8651–8665. https://doi.org/10.1007/s00253-016-7792-1
17. Spiteller, P. (2015). Chemical ecology of fungi. Natural Product Reports, 32(7), 971–993. https://doi.org/10.1039/c4np00166d
18. Park, J. M., & Forsburg, S. L. (2024). Analysis of transcriptional response in haploid and diploid Schizosaccharomyces pombe under genotoxic stress. G3 Genes Genomes Genetics, 14(9). https://doi.org/10.1093/g3journal/jkae177
19. Brown, A. J. P., Cowen, L. E., Di Pietro, A., & Quinn, J. (2017). Stress adaptation. Microbiology Spectrum, 5(4). https://doi.org/10.1128/microbiolspec.funk-0048-2016
20. Wrzosek, M., Ruszkiewicz-Michalska, M., Sikora, K., Damszel, M., & Sierota, Z. (2016). The plasticity of fungal interactions. Mycological Progress, 16(2), 101–108. https://doi.org/10.1007/s11557-016-1257-x
21. Sauters, T. J., & Rokas, A. (2025). Patterns and mechanisms of fungal genome plasticity. Current Biology, 35(11), R527–R544. https://doi.org/10.1016/j.cub.2025.04.003
22. Ishfaq, S., Anum, H., Shaheen, T., Zulfiqar, S., Ishfaq, A., Anjum, A., Ramzan, U., Rafiq, A., Mehboob-Ur-Rahman, & Guo, W. (2025). Decoding fungal communication networks: molecular signaling, genetic

 doi:10.20944/preprints202604.2000.v1

regulation, and ecological implications. Functional & Integrative Genomics, 25(1), 111. https://doi.org/10.1007/s10142-025-01620-2

23. Razo-Belmán, R., Ángeles-López, Y. I., García-Ortega, L. F., León-Ramírez, C. G., Ortiz-Castellanos, L., Yu, H., & Martínez-Soto, D. (2023). Fungal volatile organic compounds: mechanisms involved in their sensing and dynamic communication with plants. Frontiers in Plant Science, 14, 1257098. https://doi.org/10.3389/fpls.2023.1257098
24. Chen, H., Zheng, Y., Wang, M., Wu, Y., & Yao, M. (2022). Gene-Regulated Release of Distinctive Volatile Organic Compounds from Stressed Living Cells. Environmental Science & Technology, 56(13), 9546–9555. https://doi.org/10.1021/acs.est.2c01774
25. Humphris, S. (2002). The effects of volatile microbial secondary metabolites on protein synthesis in Serpula lacrymans. FEMS Microbiology Letters, 210(2), 215–219. https://doi.org/10.1016/s0378-1097(02)00604-3
26. Yaakoub, H., Mina, S., Calenda, A., Bouchara, J., & Papon, N. (2022). Oxidative stress response pathways in fungi. Cellular and Molecular Life Sciences, 79(6), 333. https://doi.org/10.1007/s00018-022-04353-8
27. Wangsanut, T., & Pongpom, M. (2022). The role of the glutathione system in stress adaptation, morphogenesis and virulence of pathogenic fungi. International Journal of Molecular Sciences, 23(18), 10645. https://doi.org/10.3390/ijms231810645
28. Park, J., & Son, H. (2024). Antioxidant systems of plant pathogenic fungi: functions in oxidative stress response and their regulatory mechanisms. The Plant Pathology Journal, 40(3), 235–250. https://doi.org/10.5423/ppj.rw.01.2024.0001
29. Črešnar, B., & Petrič, Š. (2010). Cytochrome P450 enzymes in the fungal kingdom. Biochimica Et Biophysica Acta (BBA) - Proteins and Proteomics, 1814(1), 29–35. https://doi.org/10.1016/j.bbapap.2010.06.020
30. Lah, L., Podobnik, B., Novak, M., Korošec, B., Berne, S., Vogelsang, M., Kraševec, N., Zupanec, N., Stojan, J., Bohlmann, J., & Komel, R. (2011). The versatility of the fungal cytochrome P450 monooxygenase system is instrumental in xenobiotic detoxification. Molecular Microbiology, 81(5), 1374–1389. https://doi.org/10.1111/j.1365-2958.2011.07772.x
31. Sang, H., Hulvey, J. P., Green, R., Xu, H., Im, J., Chang, T., & Jung, G. (2018). A Xenobiotic Detoxification Pathway through Transcriptional Regulation in Filamentous Fungi. mBio, 9(4). https://doi.org/10.1128/mbio.00457-18
32. Jeleń, H., Błaszczyk, L., Chełkowski, J., Rogowicz, K., & Strakowska, J. (2013). Formation of 6-n-pentyl-2H-pyran-2-one (6-PAP) and other volatiles by different Trichoderma species. Mycological Progress, 13(3), 589–600. https://doi.org/10.1007/s11557-013-0942-2
33. Harman, G. E., & Kubicek, C. P. (2002). Trichoderma and gliocladium. Volume 1. https://doi.org/10.1201/9781482295320
34. Mendoza-Mendoza, A., Esquivel-Naranjo, E. U., Soth, S., Whelan, H., Alizadeh, H., Echaide-Aquino, J. F., Kandula, D., & Hampton, J. G. (2024). Uncovering the multifaceted properties of 6-pentyl-alpha-pyrone for control of plant pathogens. Frontiers in Plant Science, 15, 1420068. https://doi.org/10.3389/fpls.2024.1420068
35. Ismaiel, A. A., & Ali, D. M. I. (2017). Antimicrobial properties of 6-pentyl-α-pyrone produced by endophytic strains of Trichoderma koningii and its effect on aflatoxin B1 production. Biologia, 72(12), 1403–1415. https://doi.org/10.1515/biolog-2017-0173
36. Garcia-Rubio, R., De Oliveira, H. C., Rivera, J., & Trevijano-Contador, N. (2020). The fungal cell wall: candida, cryptococcus, and Aspergillus species. Frontiers in Microbiology, 10, 2993. https://doi.org/10.3389/fmicb.2019.02993
37. Yoshimi, A., Miyazawa, K., Kawauchi, M., & Abe, K. (2022). Cell wall integrity and its industrial applications in filamentous fungi. Journal of Fungi, 8(5), 435. https://doi.org/10.3390/jof8050435
38. Fuchs, B. B., & Mylonakis, E. (2009). Our Paths Might Cross: the Role of the Fungal Cell Wall Integrity Pathway in Stress Response and Cross Talk with Other Stress Response Pathways. Eukaryotic Cell, 8(11), 1616–1625. https://doi.org/10.1128/ec.00193-09
39. Lu, Y., Zhu, Y., Huang, L., Pu, Y., Sun, X., Feng, J., & Sun, K. (2025). Antifungal mechanism of ketone volatile organic compounds against Pseudogymnoascus destructans. Virulence, 16(1), 2569627. https://doi.org/10.1080/21505594.2025.2569627

 doi:10.20944/preprints202604.2000.v1

40. Redza-Dutordoir, M., & Averill-Bates, D. A. (2016). Activation of apoptosis signalling pathways by reactive oxygen species. Biochimica Et Biophysica Acta (BBA) - Molecular Cell Research, 1863(12), 2977–2992. https://doi.org/10.1016/j.bbamcr.2016.09.012
41. Calvo, H., Mendiara, I., Arias, E., Gracia, A. P., Blanco, D., & Venturini, M. E. (2020). Antifungal activity of the volatile organic compounds produced by Bacillus velezensis strains against postharvest fungal pathogens. Postharvest Biology and Technology, 166, 111208. https://doi.org/10.1016/j.postharvbio.2020.111208
42. Mukherjee, P. K., Horwitz, B. A., & Kenerley, C. M. (2011). Secondary metabolism in Trichoderma – a genomic perspective. Microbiology, 158(1), 35–45. https://doi.org/10.1099/mic.0.053629-0
43. Jin, S., & Alberti, F. (2025). Advances in the discovery and study of Trichoderma natural products for biological control applications. Natural Product Reports, 42(8), 1367–1386. https://doi.org/10.1039/d5np00017c
44. Bansal, R., & Mukherjee, P. K. (2016). Identification of novel gene clusters for secondary metabolism in Trichoderma genomes. Microbiology, 85(2), 185–190. https://doi.org/10.1134/s002626171602003x
45. Hermosa, R., Cardoza, R. E., Rubio, M. B., Gutiérrez, S., & Monte, E. (2014). Secondary metabolism and antimicrobial metabolites of trichoderma. In Elsevier eBooks (pp. 125–137). https://doi.org/10.1016/b978-0-444-59576-8.00010-2
46. Flatschacher, D., Eschlböck, A., Pierson, S., Schreiner, U., Stock, V., Schiller, A., Ruso, D., Doppler, M., Ruzsanyi, V., Gründlinger, M., Büschl, C., Schuhmacher, R., & Zeilinger, S. (2025). Linking a polyketide synthase gene cluster to 6-pentyl-alpha-pyrone, a Trichoderma metabolite with diverse bioactivities. Microbial Cell Factories, 24(1), 89. https://doi.org/10.1186/s12934-025-02718-9
47. Dörfer, M., Gressler, M., & Hoffmeister, D. (2019). Diversity and bioactivity of Armillaria sesquiterpene aryl ester natural products. Mycological Progress, 18(8), 1027–1037. https://doi.org/10.1007/s11557-019-01508-z
48. Wang, Q., Cao, R., Zhang, Y., Qi, P., Wang, L., & Fang, S. (2021). Biosynthesis and regulation of terpenoids from basidiomycetes: exploration of new research. AMB Express, 11(1), 150. https://doi.org/10.1186/s13568-021-01304-7
49. Luo, P., Huang, J., Lv, J., Wang, G., Hu, D., & Gao, H. (2024). Biosynthesis of fungal terpenoids. Natural Product Reports, 41(5), 748–783. https://doi.org/10.1039/d3np00052d
50. Mózsik, L., Iacovelli, R., Bovenberg, R. a. L., & Driessen, A. J. M. (2022). Transcriptional activation of biosynthetic gene clusters in filamentous fungi. Frontiers in Bioengineering and Biotechnology, 10, 901037. https://doi.org/10.3389/fbioe.2022.901037
51. Rong, X., Zhang, L., He, W., Guo, Z., Lv, H., Bai, J., Yu, L., Zhang, L., & Zhang, T. (2024). Exploration of diverse secondary metabolites from Penicillium brasilianum by co-culturing with Armillaria mellea. Applied Microbiology and Biotechnology, 108(1), 462. https://doi.org/10.1007/s00253-024-13282-4
52. Keller, N. P. (2015). Translating biosynthetic gene clusters into fungal armor and weaponry. Nature Chemical Biology, 11(9), 671–677. https://doi.org/10.1038/nchembio.1897
53. Pennerman, K. K., Yin, G., & Bennett, J. W. (2021). Eight-carbon volatiles: prominent fungal and plant interaction compounds. Journal of Experimental Botany, 73(2), 487–497. https://doi.org/10.1093/jxb/erab438
54. Gessler, N. N., Filippovich, S. Y., Bachurina, G. P., Kharchenko, E. A., Groza, N. V., & Belozerskaya, T. A. (2017). Oxylipins and oxylipin synthesis pathways in fungi. Applied Biochemistry and Microbiology, 53(6), 628–639. https://doi.org/10.1134/s0003683817060060
55. Holighaus, G., & Rohlfs, M. (2018). Volatile and non-volatile fungal oxylipins in fungus-invertebrate interactions. Fungal Ecology, 38, 28–36. https://doi.org/10.1016/j.funeco.2018.09.005
56. Kramer, R., & Abraham, W. (2011). Volatile sesquiterpenes from fungi: what are they good for? Phytochemistry Reviews, 11(1), 15–37. https://doi.org/10.1007/s11101-011-9216-2
57. Agger, S., Lopez-Gallego, F., & Schmidt-Dannert, C. (2009). Diversity of sesquiterpene synthases in the basidiomycete Coprinus cinereus. Molecular Microbiology, 72(5), 1181–1195. https://doi.org/10.1111/j.1365-2958.2009.06717.x
58. Yingtao, L., Qiaofeng, L., Lijuan, W., Shuyun, Q., Zhou, J., Wenping, Z., & Aili, Z. (2025). Integrated analysis of transcriptomics and metabolomics and high-throughput amplicon sequencing reveals the synergistic

 doi:10.20944/preprints202604.2000.v1

effects of secondary metabolites and rhizosphere microbiota on root rot resistance in Psammosilene tunicoides. Frontiers in Microbiology, 16, 1554406. https://doi.org/10.3389/fmicb.2025.1554406

59. Pu, N., & Zhang, H. (2025). Advances in fungal promoter engineering for enhancing secondary metabolite biosynthesis. Biotechnology Journal, 20(7), e70075. https://doi.org/10.1002/biot.70075
60. Li, Q., Lin, W., Zhang, X., Wang, M., Zheng, Y., Wang, X., Gao, G., Li, Y., Zhao, D., & Zhang, C. (2024). Transcriptomics integrated with metabolomics reveal the competitive relationship between co-cultured Trichoderma asperellum HG1 and Bacillus subtilis Tpb55. Microbiological Research, 280, 127598. https://doi.org/10.1016/j.micres.2023.127598
61. Prakash, H., Karuppiah, P., Al-Dhabi, N. A., Prasad, G. S., Badapanda, C., Chakrabarti, A., & Rudramurthy, S. M. (2020). Comparative genomics of sporothrix species and identification of Putative Pathogenic-Gene determinants. Future Microbiology, 15(15), 1465–1481. https://doi.org/10.2217/fmb-2019-0302
62. Xue, P., Sánchez-León, E., Damoo, D., Hu, G., Jung, W. H., & Kronstad, J. W. (2022). Heme sensing and trafficking in fungi. Fungal Biology Reviews, 43, 100286. https://doi.org/10.1016/j.fbr.2022.09.002
63. Lara-Martínez, D., Tristán-Flores, F. E., Cervantes-Montelongo, J. A., & Silva-Martínez, G. A. (2025). Fungal stress responses and the importance of GPCRs. Journal of Fungi, 11(3), 213. https://doi.org/10.3390/jof11030213
64. Schmoll, M., Franchi, L., & Kubicek, C. P. (2005). Envoy, a PAS/LOV Domain Protein of Hypocrea jecorina (Anamorph Trichoderma reesei), Modulates Cellulase Gene Transcription in Response to Light. Eukaryotic Cell, 4(12), 1998–2007. https://doi.org/10.1128/ec.4.12.1998-2007.2005